FORMATION MECHANISM OF THREE MEMBER RING CONTAINING MICROPOROUS ZINCOSILICATE RUB-17

Ana Palčić,[1,2] Felipe Zapata Abellán,[1] Aurelie Vicente,[1] Christian Fernandez,[1] Veselina Georgieva,[1] Josip Bronić ,[2] Valentin Valtchev[1*]*

[1]Laboratoire Catalyse et Spectrochimie, ENSICAEN, Université de Caen Basse-Normandie, CNRS, 6 Boulevard Maréchal Juin, 14050 Caen, France

[2]Ruđer Bošković Institute, Bijenička 54, 10000 Zagreb, Croatia

ABSTRACT

The crystallization process of RUB-17 (RSN-type), a zeolite-type zincosilicate, was studied in order to shed light on the zeolite crystallization mechanism. The sequence of crystallization events from the formation of the initial gel to the complete transformation into a zeolite-type material was investigated. Complementary methods, including XRD, TG/dTG, Raman, ^{29}Si MAS NMR, SEM, that allowed studying both short and long-range order in the solids were used. RSN-type structure contains 3-, 4-, 5- and 6-member rings (MRs) that allowed following the formation of different building units in the course of zeolite formation. The set of experimental data revealed that the three-member ring (3MR) was the unit preferentially formed during the induction period. At this stage of gel evolution the presence of larger rings was not detected. The latter were observed only after the appearance of long-range order in the solid proved by X-ray diffraction analysis. Hence the formation of RSN-type structure was related with the large 3MRs population during the induction stage.

INTRODUCTION

Zeolites and related materials are crystalline solids with well-defined system of channels and/or cavities with size below 2 nm. The elementary building unit is TO_4 tetrahedron (T = Si, Al, Ge, Ga, P, Ti, …). The tetrahedral units are connected via four common oxygen atoms thus forming a three-dimensional framework. Up to now, there are 229 zeolite framework types approved by the structure commission of International Zeolite Association.[1] Due to their large structural and compositional diversity, zeolites have different physicochemical properties. They are widely used in modern society with applications ranging from household to chemical process industry. Their most important applications are in the fields of

heterogeneous catalysis, gas separation and ion exchange.[2] Besides in petroleum refining and petrochemistry, the catalytic and separation properties of zeolites are used in emerging fields as processing of renewable and alternative feedstocks, pollution abatement, energy saving, as well as in chemical sensing.[3] Hence, the advances in this domain of material science are of vital importance in order to face new technological challenges, but also to provide more efficient solutions than the already existing ones. Thus, both new materials and modified well-known zeolite molecular sieves are highly desired in order to address the nowadays needs.

Diffusion limitations in micropore channels decrease the efficiency of crystalline microporous materials. There are two fundamentally different approaches that are used to address this issue: i) the preparation of zeolite crystal containing a supplementary system of larger (meso-)pores; and ii) the synthesis of new zeolites with extra-large pores, i.e., pores larger than 7-8 Å.

Based on theoretical studies, Brunner and Meier postulated that zeolite structures built up of small rings, namely 3 and 4 member rings (MR), are expected to exhibit lower framework density.[4] At that time, the only known zeolitic material containing 3-member rings was the beryllium containing mineral lovdarite (LOV-type). In this structure, two 3-member rings sharing one vertex thus composing a unit named *lov* (*spiro*-5) (see Supplementary Information, S1a).[1] Soon after that paper, the synthesis of the aluminosilicate material ZSM-18 (MEI-type) with 3-member ring was reported.[5] As far as we know, this is the only three-member ring containing aluminosilicate zeolite.[6] Thereafter, several new 3-member ring containing zeolitic materials were synthesized by the incorporation of heteroatoms as Be, Zn, Li and Ge in the zeolite framework.[7,8] The use of Ge allowed Corma and co-workers to synthesize a number of extra-large pore zeolites containing double four- and double three-member rings. Some of these structures exhibited the lowest known framework densities amongst silica-based zeolites.[9] Three-member ring zeolite structures are usually formed when Al is replaced by cations that offer higher flexibility of T-O bond angle and thus formation of smaller ring units. Three-member rings can also be found in pure vitreous silica systems as well as when Al is added to the glasses.[10] Recently, a theoretical study showed that a 3MR in IRR-type framework could be built exclusively of Ge or Si atoms.[11] The latter study also revealed that the introduction of Zn in the double 3-member ring reduces the steric constraints of the framework.

The position of heteroatoms in 3MR containing molecular sieves is relatively well studied. For instance, the location of Al in the framework of ZSM-18 is well known.[5] In

spiro-5 units, which built the structures of lithosilicates RUB-23 and RUB-29, lithium is situated in the *spiro* position while Si is at the vertices.[12,13] Beryllium when found in *lov* units can be located both in the *spiro* center and at the vertices.[7,14] On the other hand, Zn in the *lov* unit of VPI-7 is exclusively located at the vertices.[15,16] Although without any doubt the Zn is situated in 3MR of RSN-type structure, its exact position is not known.

The zincosilicate RUB-17 (RSN-type) is a three-member ring containing zeolitic material (see Supplementary Information, S1b).[17] The RSN framework is composed of 3-, 4-, 5-, 6-member rings arranged in a way to form a tridimensional system of channels 9 (3.3×4.4 Å) × 9 (3.1×4.3 Å) × 8 (3.4×4.1 Å). The structure exhibits C1m1 space group, unit cell parameters a = 7.238 Å, b = 40.56 Å, c = 7.308 Å, α = 90, β = 91.8 and γ = 90. The idealized unit cell composition of RUB-17 is $K_4Na_{12}[Si_{28}Zn_8O_{72}]\cdot 18H_2O$.

RUB-17 is a small pore zeolite that might find application in the separation of small molecules and as an ion-exchanger. Zinc is a biogenic chemical element, which makes RUB-17 an environment friendly material. The RSN-type structure could also be interesting for catalytic and sensing applications.[18,19] For any potential usage, thorough characterization of material is crucial, especially the positions of different cations in the framework because it has a direct impact on the physicochemical properties.

Zeolites are already 50 years produced on a large scale and used in number of chemical processes. The main crystallization steps one zeolite yielding system passes through are well recongnized.[20] However, the crystallization pathway may differ depending on the initial system employed. In addition the molecular level mechanism and the species participating in the nucleation/crystallization process are not well studied. Both, *ex situ* and *in situ* methods, are used and often combined in order to shed more light in zeolite formation.[21-25] Substantial progress has been made, however there is still not a clear picture on the precursor species participating in the zeolite formation, in particular during the nucleation stage.[26,27]

The objective of present study is to establish a relationship between the precursor units in the initial gel and the zeolite structure formed. Performed experiments were executed *ex situ*, i.e., the reaction was quenched at different stages and the recovered solid phase washed. A disadvantage of this approach is that units formed in mother liquor are washed out and only the solid part of the system is subjected to analysis. In addition, the precursor units are not studied in their natural environment. On the other hand, this approach allows solely units that are abundant and stable enough to be studied. Moreover, the *in situ* method used up to know did not point out clearly the species that participate in zeolite nucleation process. In order to determine the stable species that survive the post-synthesis treatment we have employed

methods as Raman and ^{29}Si NMR spectroscopy that provide information for the short range order in the materials. Theoretical calculations have also been used to shed more light on silicon NMR spectra. The ultimate goal was to define the location of Zn atoms in 3MR units, which would allow tracking down the formation of these units in the course of crystallization process.

EXPERIMENTAL PART

To prepare the reaction mixture, 0.57 g of zinc oxide (powder, 99%, Prolabo), 1.44 g of sodium hydroxide (pellets, 97%, Sigma Aldrich), 2.30 g of potassium hydroxide (pellets, 97%, Sigma Aldrich), 2.08 g of tetraethylammonium hydroxide (35% water solution, Aldrich), and 53.43 g of distilled water were mixed and treated in an ultrasonic bath for 30 min. Finally, 15 g of tetraethoxysilane (98%, Sigma Aldrich) was added to the mixture. The final molar oxide composition of the initial gel was: 1.00TEOS:0.10ZnO:0.50NaOH:0.50KOH:0.08TEAOH:44.00H_2O. The synthesis was performed at 483 K for different periods of time. In order to follow the crystallization of RUB-17 the crystallization time (t_c) was varied between 8 and 222 h. The liquid phase of every sample was separated, while the solid phase was washed with distilled water and dried at 353 K. The yield is 40 wt% in respect to SiO_2.

X-ray diffraction (XRD) patterns of the solid phases were collected by PANalytical X'pert PRO MPD diffractometer using Cu-K_α monochromatic radiation (λ = 1.5418 Å, 45 kV, 40 mA) and used for the qualitative and quantitative phase analysis. The samples were scanned in the range of Bragg's angles 2θ = 5-50°, step size 0.0167°, time per step 99.68 s. Thermal analyses of the solid phases were performed by Setaram Setsys TGA instrument. The samples were heated up to 1073 K by rate 5 K/min in air flow. MIRA-LMH (Tescan) scanning electron microscope equipped with field emission gun was employed to obtain scanning electron micrographs (SEM). Raman spectra of the samples were measured using Jobin Yvon Labram 300 spectrometer equipped with a confocal microscope. The measurements were done using a He-Ne laser having the wavelength of 632.8 nm. The spectra were taken for 60 s and accumulated 5 times.

^{29}Si MAS NMR spectra were recorded at 99.3 MHz on a Bruker Avance III (11.7 T) spectrometer using 4 mm-OD zirconia rotors and a spinning frequency of 12 kHz. To account for the long T_1 relaxation of ^{29}Si, a single pulse excitation (30° flip angle) was used with a recycling delay of 60 s. Tetramethylsilane (TMS) was used as chemical shift reference.

The calculation of ^{29}Si MAS NMR spectrum was carried out with density functional

theory (DFT) using the CASTEP (version 6.0) code and Gauge Including Projector Augmented Wave (GIPAW) method.[28-30] The input data were the crystallographic atomic positions of RUB-17 obtained from the IZA structural database.[1] "On-the-fly" (OTF) ultra-soft pseudo-potentials generated by CASTEP, Perdew-Burke-Ernzerhof (PBE) functional, a cut-off energy of 100 Ry and a k-point spacing of 0.125 $Å^{-1}$ were employed for the calculations.[31] Before computing the isotropic electronic shieldings, a geometry optimization (with fixed unit cell) of the structure was performed using the quasi-Newton Broyden-Fletcher-Goldfard-Shanno (BFGS) method.[32]

RESULTS AND DISCUSSION

General characterization

The XRD pattern of the solid obtained after 8 h of hydrothermal treatment showed the presence of zinc oxide and a *halo* indicative of the presence of amorphous phase (Figure 1). The amount of ZnO in the solid phase progressively decreased and ZnO peaks disappeared after 120 h of hydrothermal treatment. The first traces of crystalline RSN-type material were detected after 28 h of hydrothermal treatment. According to the crystallization curve calculated on the grounds of the XRD patterns, the solid was fully crystalline after 222 h.

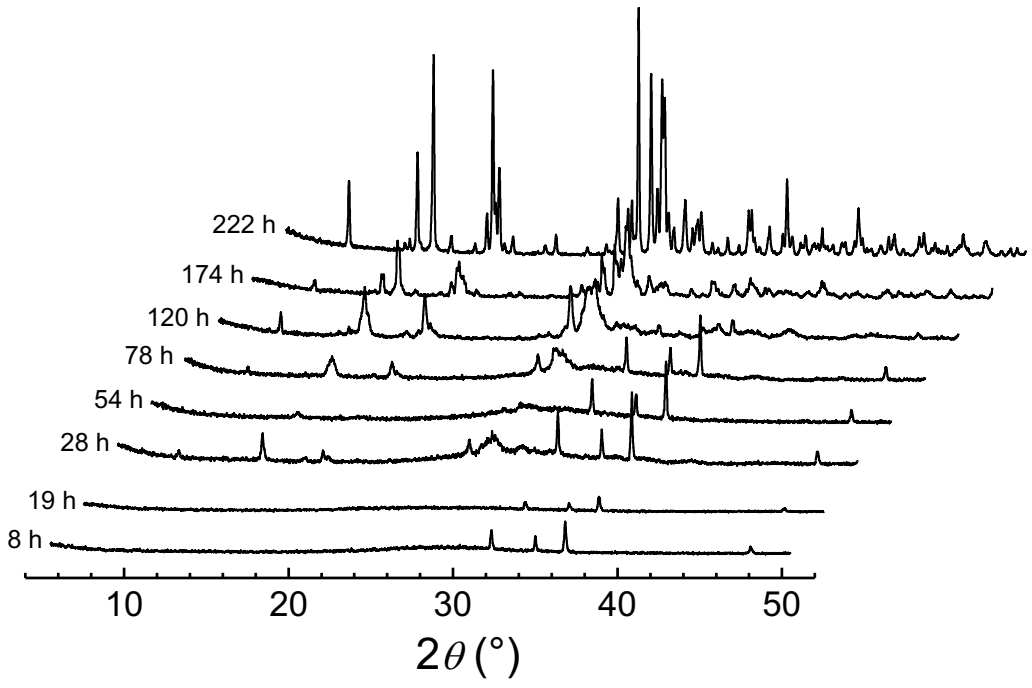

Figure 1. XRD patterns of the series of samples taken during the RUB-17 synthesis.

According to the SEM inspection (Figure 2) the size of RUB-17 crystals is not uniform ranging between 100 and 1500 nm. The morphology of individual crystals varies from long to short prismatic. Most of the crystals are intergrown forming aggregates of different size.

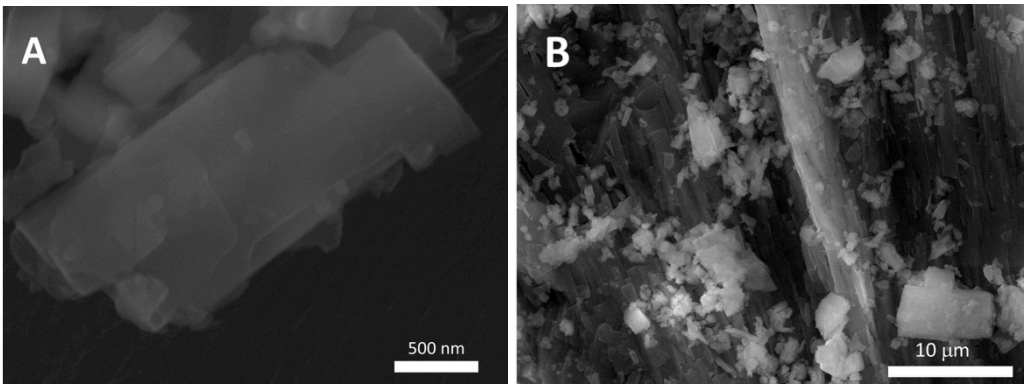

Figure 2. SEM micrographs of the RUB-17 crystals obtained at 180 °C after 222 h of hydrothermal treatment.

Röhrig and Gies reported that RUB-17 exhibits low structure stability. The framework collapsed at 220 °C after 24 h heating. They noted the critical role of water molecules and alkali metal cations in the stabilization of RUB-17.[17] Our TG/dTG analysis of a fully crystalline RUB-17 shows that the occluded water is released in the temperature range 25 – 400 °C (Figure 3). There are two major dehydration steps, as during the first one with a maximum at 199 °C, 6.2 wt. % of water is released, corresponding to 11 molecules of water. A second maximum is centered at 286 °C and then 7 molecules of water are let out. The first event is exothermic while the second is endothermic (DSC curve shown in Supplementary Information, Figure SI-2). The total amount of released water is 10.1 wt. %, which corresponds well to the unit cell composition (18 molecules of water).[17] Generally, the zeolite-type water is released substantially below 200 °C. Therefore we attribute the first weight loss to zeolite type water. The second weight loss, which is completed at about 400 °C, is related with much stronger interactions. Obviously these are the water molecules that stabilize the zeolite framework. This suggestion is supported by the fact that during their release the structure of RUB-17 collapses. The exact position of these molecules can only be obtained by a structural study, which is out of the scope of present investigation.

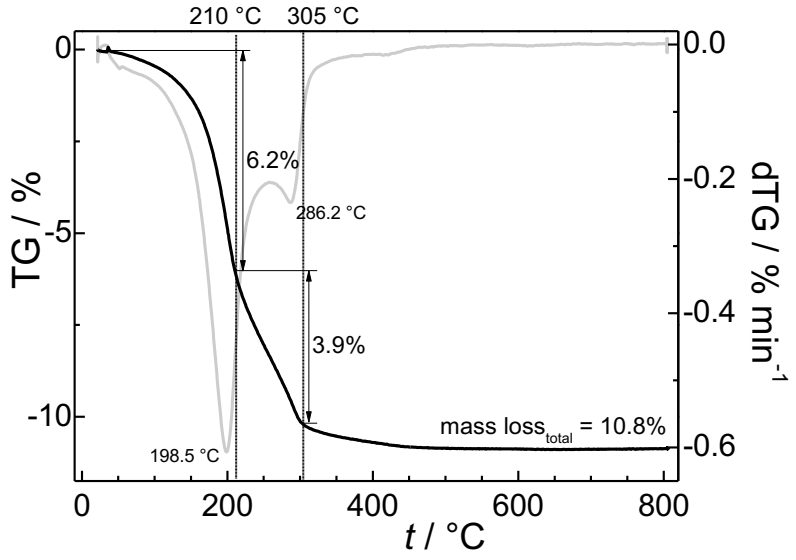

Figure 3. TG and dTG curves of highly crystalline RUB-17.

Crystal growth kinetics

XRD study shows that the process of RUB-17 formation is relatively slow. Although the first diffraction peaks appear after 28 h, fully crystalline material is obtained only after 222 h. We attribute the extended crystal growth process to the slow dissolution of Zn source. For better understanding of the formation of RUB-17, the solid phases recovered during different stages of the reaction were subjected to TG analysis (Figure 4). The zinc oxide used as a starting material was also analyzed. It exhibits only one endothermic weight loss (1.9 wt. %.) step with maximum at 249 °C. The observed signal is most probably due to water coordinated to the metal oxide. The sample taken after 8 h of hydrothermal treatment contains the largest amount of water, which is about 14.5 wt. %. With the increase of crystallinity the water content decreases gradually and reaches 10.1 wt. % in the highly crystalline material. Higher water content in the amorphous and partially crystalline solids is attributed to the interaction between water and silanol groups in the amorphous phase. In the course of zeolite framework formation a condensation of chemical bonds Si–O–Si(Zn) takes place, which is coupled with release of loosely attached water. The results of TG analysis are in full agreement with the XRD study and can be used to follow the crystallization process.

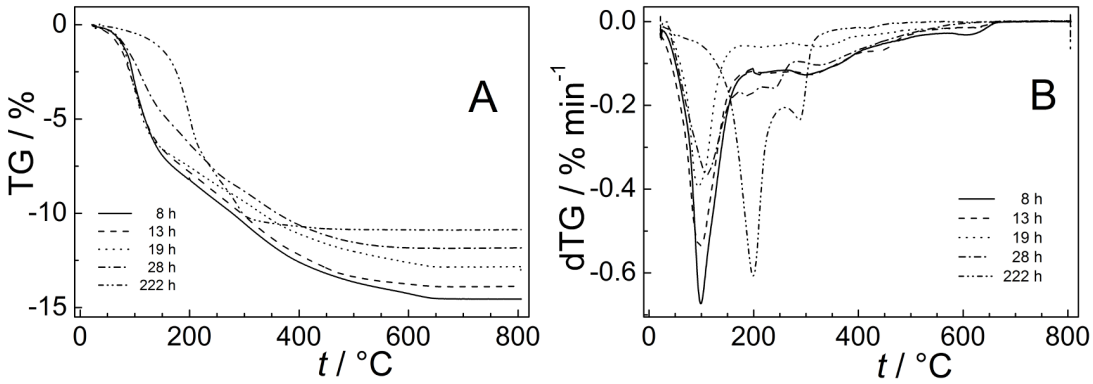

Figure 4. TG (A) and dTG (B) curves of the solid samples taken in the course of RUB-17 crystallization.

The crystal growth kinetics of RUB-17 has also been tracked by Raman spectroscopy. The most intense Raman bands of ZnO are at 150, 438 and 1068 cm^{-1} (Figure 5A). A significant change in the Raman spectra takes place after 28 h of hydrothermal crystallization when the characteristic bands of new phase appear. For instance, wide maxima ranging from 310 to 365 cm^{-1} and 1030 to 1120 cm^{-1} as well as peaks at 440, 456, 497, 519, 587 and 662 cm^{-1} can be seen (Figure 5A). With the increase of crystallization time the bands become sharper.

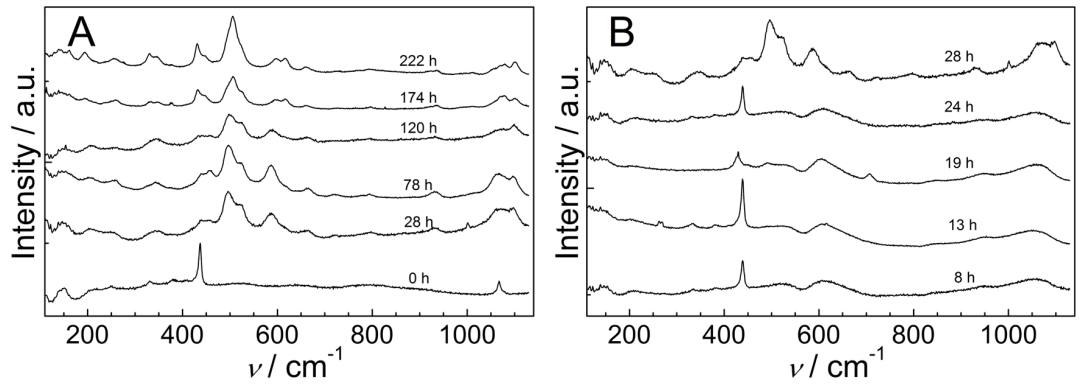

Figure 5. Crystal growth kinetics of RUB-17 followed by Raman spectroscopy (A) and the spectra taken during the induction period (8 – 28 h) when no crystalline material was detected (B).

Similarly to other zeolite-type materials the spectra of RUB-17 exhibits the most intense bands in the 300 – 600 cm^{-1} range. In this region the bands corresponding to small ring building units are usually visible. On the grounds of a previous study the peaks in the range 550 – 620 cm^{-1}, 470 – 530 cm^{-1} and 370 – 430 cm^{-1} were attributed to 3-, 4- and 5-member

rings, respectively.[33] Six member rings usually exhibit a band in the region 290 – 410 cm^{-1}, whereas larger rings have a band below 290 cm^{-1}.[34] A closer look at the Raman spectra taken between 8 and 28 h of hydrothermal treatment revealed the presence of organized units in amorphous precursor (Figure 5B). Namely, there is a clear distinction between the initial gel and the solid phase recovered after 8 h of hydrothermal treatment. The later exhibits wide Raman maxima in the regions 565 – 700 and 990 – 1115 cm^{-1}. In the samples taken after 13, 19 and 23 h these regions evolve to the bands of RUB-17 corresponding to 3-member rings, with maxima at 597 and 615 cm^{-1} and also unassigned asymmetric stretching motion bands at 1079 and 1102 cm^{-1}. On the other hand, during this early stage of zeolite formation there are not any signs of the presence of 4-, 5- and 6-member rings. Obviously during the induction period the 3-member rings are the dominating units in the amorphous, while if there are any larger (4-, 5- and 6-) rings they are below the detection limit of the Raman method. We relate this fact with the presence of Zn in the reaction system that favors the formation of 3MR. A gradual increase of the number of these units is observed in the Raman spectrum of the samples taken between 8 and 24 h, which certainly influence the reactions in the system and in particular the nucleation process. After 28 h of hydrothermal treatment the first traces of zeolite structures are detected by XRD analysis. Simultaneously with the first traces of crystalline RSN-type zeolite the bands of 4MR (505 and 528 cm^{-1}), 5MR (431 and 445 cm^{-1}) and 6MR (330 and 343 cm^{-1}) rings appear in the Raman spectrum (Figure 5B). Based on these results one can state that the long-range order is observed only after reaching a critical concentration of 3MR units in the precursor. Similar results were reported on the crystallization of zeolite A, for which Raman and NMR spectra indicated the formation of D4R in the early stage of the reaction, while 6MR were observed simultaneously with the appearance of crystalline phase.[35]

The ^{29}Si MAS NMR spectrum of the fully crystalline RUB-17 is shown on Figure 6A. Assuming identical shapes and widths for all lines, seven distinct resonances are needed to fit this spectrum. They most probably correspond to the seven non-equivalent T sites of the RSN framework. Among these resonances, a single well-resolved peak can be observed at -82.2 ppm, the other peaks range between -92 and -95 ppm. Röhrig and Gies attributed the peak at -82 ppm to a silicon atom located in the center of the *lov* unit, which chemical shift could be due to the vicinity of two Zn atoms.[17] Later, Camblor and Davis found similar chemical shift in another zeolite-type zincosilicates.[16]

In order to validate the above attributions and to determine the most probable location of the Zn in the *lov* unit, we have performed a DFT calculation of the ^{29}Si chemical shifts. First a

geometry optimisation, electronic energy calculation was carried out based on the data obtained from the IZA database. The geometry optimization was also done using a hypothetical structure containing two Zn in a single 3MR. This configuration leads to energy 11 eV higher than that with a single Zn in each 3MR, which is in agreement with previous literature data.[16] The isotropic ^{29}Si MAS NMR electronic shielding's were thus calculated on the most probable structure with a Zn in each 3MR. Although water molecules linked to the framework may have some important effect, we were not considering them in these calculations as the geometry optimisation was requiring too much computational time. The accuracy of our calculations can be checked by comparing our data with the correlation between calculated and observed chemical shifts for a large series of silicates as given by Cadars *et al*.[36] The calculated *versus* experimental data are displayed on Figure 6B. Unambiguously, our results fit well this correlation except for the resonance at -82 ppm, which is off by about 3 ppm. The apparent disagreement can be easily explained first by the fact that we do not take into account the water molecules, and second that the optimization was done using a fixed cell. More comprehensive investigation is required to really assign the NMR spectrum, which is out of the scope of this paper. However, the calculation shows that the -82 ppm line corresponds to the Si atom located in *spiro* position (between two 3-member rings) and it is surrounded by two Zn atoms: Q_4(2Zn). The six other lines are the other silicons, which are all close to one Zn: Q_4(1Zn).

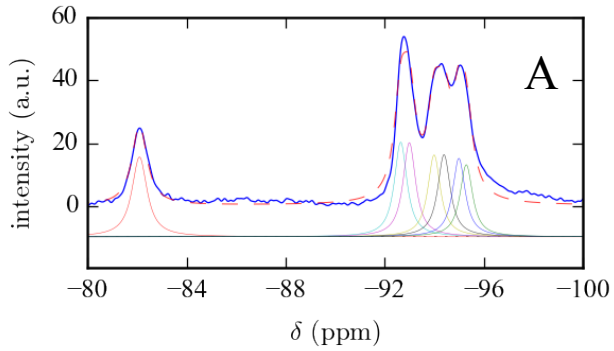

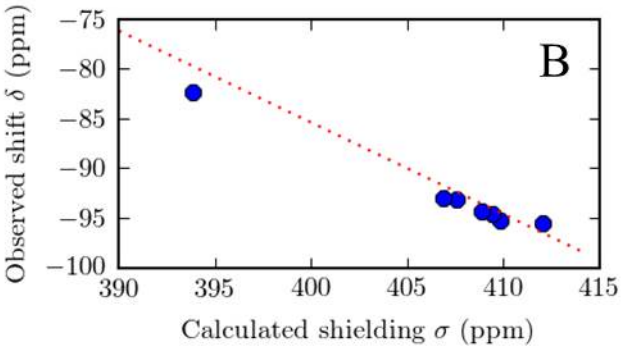

Figure 6. ^{29}Si MAS NMR spectrum of RUB-17: A) experimental spectrum, its decomposition assuming 7 distinct Si sites and the decomposition sum in dotted line; B) relationship between the list of shieldings calculated with CASTEP and that of the observed shifts; both lists are ordered by increasing values. The dotted red line reproduces the expected correlation as published by Cadars *et al*., i.e., $\delta\left(^{29}Si\right) = -0.922\sigma + 283.39$.[36]

The crystal growth of RUB-17 was also studied by ^{29}Si MAS NMR technique. The sample taken after 8 h of the hydrothermal treatment exhibits a wide maximum spreading from -72 to -105 ppm (Figure 7). This result supports the formation of bonds Zn–O–Si and Si–O–Si after 8 h of hydrothermal treatment, but it also indicates that some organized units are already formed in this early crystallization stage. After 13 h hydrothermal treatment a maximum at about -82 ppm can be observed. As stated already, this line corresponds to the Si atom located in *spiro* position. After 40 h a second well pronounced maximum between -92 ppm and - 97 ppm appears in the spectrum. With the advancement of the reaction the two maxima get narrower and after 54 h of hydrothermal treatment two peaks at about -80 and -95 ppm become distinguishable. The relative intensity is increasing with the reaction time and after 222 h of hydrothermal treatment well-resolved peaks can be observed.

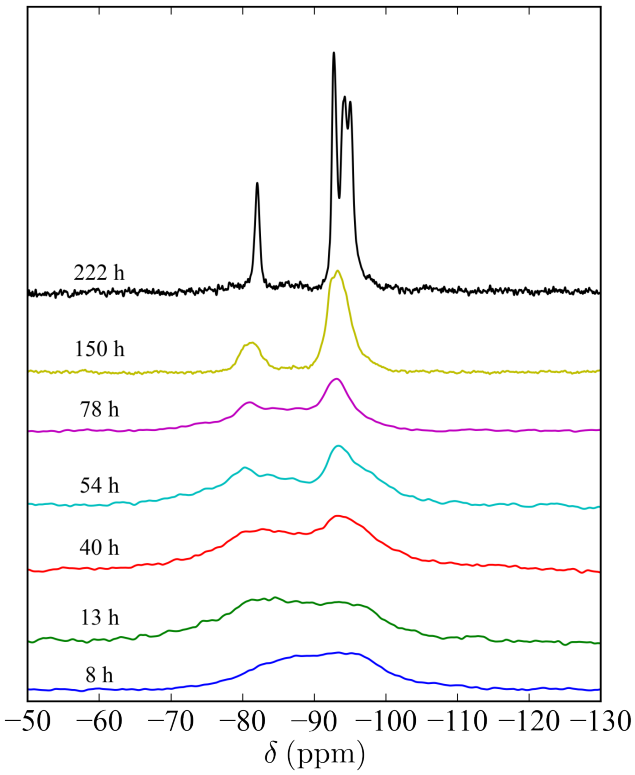

Figure 7. Crystal growth kinetics of RUB-17 followed by ^{29}Si MAS NMR.

The framework of RSN-type zeolite comprises 3-, 4-, 5- and 6-member rings. Actually, the framework contains all small rings that can be found in a zeolite structure. In addition, it is well known that the Zn atoms are situated in 3MR. These particularities of RSN-type framework offer the opportunity to study and discriminate the building units formed during different stages of zeolite formation and in particular during the induction period, which is crucial for the nucleation process. During the induction period large numbers of different nuclei are formed, but a few of them cross the energetic barrier and become crystals. In order to become viable and continue growing a nucleus has to be in equilibrium with the surrounding nutrient pull.

The analysis of initial system prior to the hydrothermal treatment did not reveal the presence of ring structures in the solid. The three-member ring was the first organized unit detected during the induction stage. This suggests that the mass of these units is over the detection limit of Raman spectroscopy. Their concentration rapidly increased between 8 and 28 h of hydrothermal treatment. Only after the appearance of first crystalline material the presence of larger (4-, 5- and 6-) rings were detected. The increase of the concentration of 4-, 5- and 6-member rings correlates with the crystallinity of the solid.

Zeolite nucleation process includes numerous equilibriums and condensation steps. It is indeed difficult to distinguish which of quasi-stable intermediate structure is critical for the formation of a particular zeolite. In the present study the only stable unit that can be detected during the induction period is the 3MR. It is noteworthy that the concentration of this units increases during the induction period. In contrast, the concentration of larger ring units correlates with the crystallinity of the product. Hence, we relate the high concentration of 3MR during the induction period with the nucleation of this framework type. One may argue that the abundance of this unit during the induction stage is not critical for RSN-type framework formation. It is worth recalling, however, that the 3MR is a key unit for RSN-type structure since two connected 3MR rings build the *lov* building unit. Taking into consideration that the only known material with RSN framework is zincosilicate RUB-17, we can state that the presence of Zn is crucial for the formation of 3MR under employed synthesis conditions and hence the formation of RSN structure.

CONCLUSION

The crystal growth kinetics of the microporous zincosilicate RUB-17 was studied. Fully crystalline material was obtained after 222 h of hydrothermal crystallization. The solids obtained at different stages of zeolite formation were subjected to characterization by different physical methods in order to get insight in crystal growth mechanism.

The detailed analysis of the induction period showed a gradual decrease of the content of ZnO. This process was coupled with the formation of three member ring units, which were clearly detected by Raman and ^{29}Si MAS NMR spectroscopy. Larger ring (4-, 5- and 6-) units were not observed during the induction period. The increase of the concentration of larger rings correlates with the appearance of long range order in the solid. These data clearly show that the zeolite formation depends on the concentration of a particular unit during the induction stage that governs the crystallization process to a particular framework type. In the case of RUB-17 these are the 3MR that are preferentially formed during the induction stage and govern the nucleation process.

ACKNOWLEDGMENTS

The authors acknowledge the MicroGreen project (ANR-12-IS08-0001-01) and the Lower Normandy Region (France) for the financial support. Financial support for the NMR equipment from both Labex EMC_3 (ANR) and FEDER is gratefully acknowledged.

REFERENCES

1 http://www.iza-structure.org/ (15/07/2015)

2 L.B. McCusker, C. Baerlocher, *Stud. Surf. Sci. Catal.*, 2001, **137**, 37-67.

3 J.-P. Gilson, O. Marie, S. Mintova, V. Valtchev, in *Zeolites and Ordered Porous Solids: Fundamentals and Applications*, C. Martinez, J Perez-Pariente (Eds.), Universitat Politecnica de Valencia, 2012.

4 G.O. Brunner, V.M. Meier, *Nature*, 1989, **337**, 146-147.

5 S.L. Lawton, W.J. Rohrbaugh, *Science*, 1990, **247**, 1319-1322.

6 G. Wang, B. Marler, H.Gies, C.A. Fyfe, P. Sidhu, B. Yilmaz, U. Müller, *Micropor. Mesopor. Mater.*, 2010, **132**, 43-53.

7 A.K. Cheetham, H. Fjellvåg, T.E. Gier, K.O. Kongshaug, K.P. Lillerud, G.D. Stucky, *Stud. Surf. Sci. Catal.*, 2001, **135**, 788-795.

8 J. Jiang, J.L. Jorda, M.J. Diaz-Cabañas, J. Yu, A. Corma, *Angew. Chem. Int. Ed.*, 2010, **49**, 4986-4988.

9 A. Corma, M.J. Díaz-Cabañas, J. Jiang, M. Afeworki, D.L. Dorset, S.L. Soled, K.G. Strohmaier, *PNAS*, 2010, **107**, 13997-14002.
10 C. Le Loq, D.R. Neuville, P. Florian, G.S. Henderson, D. Massiot, *Geochim. Cosmochim. Acta*, 2014, **126**, 495-517.
11 P. Petkov, H. Aleksandrov, V. Valtchev, G. Vayssilov *Chem. Mater.*, 2012, **24**, 2509-2518.
12 S.-H. Park, P. Daniels, H. Gies, *Micropor. Mesopor. Mater.*, 2000, **37**, 129-143.
13 S.-H. Park, M. Kleinsorge, C.P. Grey, J.B. Parise, *J. Solid State Chem.*, 2002, **167**, 310-323.
14 J.A. Armstrong, M.T. Weller, *J. Am. Chem. Soc.*, 2010, **132**, 15679-15686.
15 C. Röhrig, I. Dierdorf, H. Gies, *J. Phys. Chem. Solids*, 1995, **56(10)**, 1369-1376.
16 M.A. Camblor, M.E. Davis, *J. Phys. Chem.*, 1994, **98**, 13151-13156.
17 C. Röhrig, H Gies, *Angew. Chem. Int. Ed.*, 1995, **34**, 63-65.
18 K. Wetchakuna, T. Samerjaia, N. Tamaekonga, C. Liewhirana, C. Siriwonga, V. Kruefua, A. Wisitsoraatb, A. Tuantranont, S. Phanichphant, *Sens. Actuators B*, 2011, **160**, 580-591.
19 J. Strunk, K. Kähler, X. Xia, M. Muhler, *Surf. Sci.*, 2009, **603**, 1776-1783.
20 C. S. Cundy, P. A. Cox, *Micropor. Mesopor. Mater.*, 2005, **82**, 1-78.
21 C. S. Cundy, P. A. Cox, *Chem. Rev.,* 2003, **103**, 663-702.
22 A. I. Lupulescu, J. D. Rimer, *Science*, 2014, **344**, 729-732.
23 I.H. Lim, W.Schrader, F.Schüth, *Micropor. Mesopor. Mater.*, 2013, **166,** 20-36**.**
24 J. D. Rimer, M. Kumar, R. Li, A. I. Lupulescu and M. D. Oleksiak, *Catal. Sci. Techn.,* 2014, **4**, 3762-3771.
25 F. Fan, Z. Feng, C. Li, *Chem. Soc. Rev*., 2010, **39**, 4794–4801.
26 M. Smaihi, O. Barida, V. Valtchev, *Eur. J. Inorg. Chem.*, 2003, 24, 4370–4377.
27 L. Itani, Y. Liu, W.P. Zhang, K.N. Bozhilov, L. Delmotte, V. Valtchev, *J Am. Chem. Soc.*, 2009, **131**, 10127–10139.
28 S.J. Clark, M.D. Segall, C.J. Pickard, P.J. Hasnip, M.J. Probert, K. Refson, M.C. Payne, *Z. Kristallogr.*, 2005, **220**, 567-570.
29 M.D. Segall, P.J.D. Lindan, M.J. Probert, C.J. Pickard, P.J. Hasnip, S.J. Clark, M.C. Payne, *J. Phys-Condens. Mater.*, 2002, **14**, 2717-2744.
30 C. Bonhomme, C. Gervais, F. Babonneau, C. Coelho, F. Pourpoint, T. Azais, S.E. Ashbrook, J.M. Griffin, J.R. Yates, F. Mauri, C.J. Pickard, *Chem. Rev.*, 2012, **112**, 5733-5779.

31 Perdew, J.; Burke, K.; Ernzerhof, M. *Phys. Rev. Lett.*, 1996, **77***,* 3865-3868.
32 J. D. Head, M. C. Zerner. *Chem. Phys. Letters*, 1985, **122**, 264-270.
33 P.K. Dutta, D.C. Shieh, M. Puri, *Zeolites*, 1988, **8**, 306-309.
34 Y. Yu, G. Xiong, C. Li, F.-S. Xiao, *Micropor. Mesopor. Mater.*, 2001, **46**, 23-34.
35 L. Ren, C. Li, F. Fan, Q. Guo, D. Liang, Z. Feng, C. Li, S. Li, F.-S. Xiao, *Chem. Eur. J.*, 2011, **17**, 6162-6169.
36 S. Cadars, M. Allix, D.H. Brouwer, R. Shayib, M. Suchomel, M.N. Garaga, A. Rakhmatullin, A.W. Burton, S.I. Zones, D. Massiot, B.F. Chmelka, *Chem. Mater.*, 2014, **26**, 6994–7008.